Mobilities of NO + drifting in helium: A molecular dynamics study

R. Baranowski and M. Thachuk

Citation: The Journal of Chemical Physics **110**, 11383 (1999); doi: 10.1063/1.479079
View online: http://dx.doi.org/10.1063/1.479079
View Table of Contents: http://scitation.aip.org/content/aip/journal/jcp/110/23?ver=pdfcov
Published by the AIP Publishing

Mobilities of NO^+ drifting in helium: A molecular dynamics study

R. Baranowski and M. Thachuk[a)]
Chemistry Department, University of British Columbia, Vancouver V6T 1Z1, Canada

(Received 1 February 1999; accepted 25 March 1999)

A new molecular dynamics (MD) method is introduced, and used to study NO^+ ions drifting in helium under the influence of a uniform electric field. Mobilities, average values of squared velocities, and self-diffusion coefficients parallel and perpendicular to the electric field are reported for two recent *ab initio* potential surfaces: a coupled cluster singles–doubles with perturbative treatment of triple excitations [CCSD(T)] surface [S. K. Pogrebnya *et al.*, Int. J. Mass Spectrom. Ion Processes **149/150**, 207 (1995)] and a MP4SDTQ/6-311+G($2df,p$) surface [L. A. Viehland *et al.*, Chem. Phys. **211**, 1 (1996)]. Average values of angular momentum and alignment parameters are also reported and compared. In all cases, no significant differences were found in the calculated values for the two different potential surfaces. Finally, mobility values are compared with experimental measurements [J. A. de Gouw *et al.*, J. Chem. Phys. **105**, 10398 (1996)] and good agreement is obtained for both potential surfaces. © *1999 American Institute of Physics.* [S0021-9606(99)51623-1]

I. INTRODUCTION

Gas-phase ion mobilities have been of interest for many years. Mobility measurements combined with theoretical investigations and other transport properties allow aspects of the ion-bath gas interaction to be determined, and these in turn can be related to the geometry and structure of an ion. At present a large quantity of data is available on the mobility of atomic and simple molecular ions in a variety of buffer gases.[1] The transport properties of ions have been studied experimentally, mainly utilizing drift tube experiments,[1] and theoretically with the momentum transfer method, the moment solution of the Boltzmann equation,[1,2] as well as with Monte Carlo[3,4] and molecular dynamics studies.[5]

Because mobilities depend upon the overall size, shape, and charge distribution of the ion, studies of complex ions and their transport properties have attracted a lot of attention in the last few years. Jarrold *et al.*[6,7] have measured the mobilities of a number of metal and carbon cluster ions, from which classes of isomers with different shapes were identified. Bowers *et al.*[8,9] use mobility measurements to differentiate the conformations of some biological molecules. In addition, Douglas and co-workers[10,11] have used kinetic energy loss measurements to study a variety of protein ions.

The interpretation of the transport data for these larger systems is based upon an estimation of a temperature dependent momentum-transfer cross section. More rigorous and accurate approaches based upon solution of the Boltzmann equation[1] have been restricted mainly to atomic systems. Recently, this level of theory has been applied to molecular ion systems.[12,13] The main idea in these approaches involves an expansion of the ion velocity distribution function, relying upon a sufficiently rapid convergence. In recent theoretical studies of NO^+ drifting through helium, Viehland *et al.*[14] observed poor convergence at intermediate field strengths, and transport properties were calculated in the weak field limit only.

In the present study, an alternative approach based upon a molecular dynamics (MD) technique is developed. Mobilities, diffusion coefficients parallel and perpendicular to the electric field, and velocity autocorrelation functions are calculated for two recent potential energy surfaces,[14,15] and compared with a previous theoretical calculation[14] and experimental results.[16] This study probes the sensitivity of the ion-bath gas interaction on mobilities and on collision-induced alignment.

The paper is organized as follows. Section II describes the potential surfaces for NO^+–He, while Sec. III details the molecular dynamics procedure. Results are presented and compared to theoretical results and experimental data in Sec. IV, with final conclusions and comments following in Sec. V.

II. POTENTIAL ENERGY SURFACE FOR NO^+–HE

A semiempirical potential energy surface for NO^+–He system was constructed by Zenevich *et al.*[17] to calculate rate constants for vibrational relaxation. Since then, two new *ab initio* calculations of NO^+–He have been published.

Pogrebnya *et al.*[15] employed the coupled cluster singles–doubles method with perturbative treatment of the triple excitations [CCSD(T)] to determine a potential surface in the study of the vibrational relaxation of NO^+ in helium. The equilibrium NO bond length was calculated to be $2.0091a_0$, and this was the value used in the present calculations for this potential. The minimum of the NO^+–He complex had a well depth of $8.49\times10^{-4}E_h$ and was located at $R=5.291a_0$ and $\theta=100.2°$, where R is the distance from the center-of-mass of NO to the helium atom, and θ is the angle of the helium atom measured from the NO bond axis (a_0 is the Bohr radius, E_h is the Hartree energy). The linear

a)Electronic mail: thachuk@chem.ubc.ca

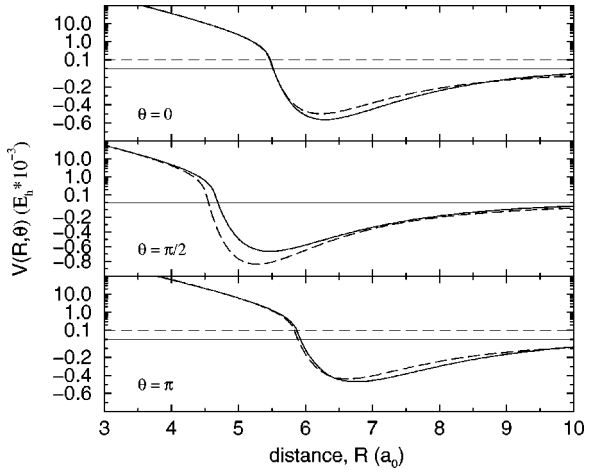

FIG. 1. Comparison of the potential surfaces as a function of R for NO^+–He at three orientations. The solid curve represents the potential surface of Ref. 14, while the dashed curve represents the potential surface of Ref. 15. Note that the scale of the ordinate in each graph changes from linear to logarithmic above the dashed horizontal line.

configuration with the helium next to nitrogen corresponds to $\theta=0$.

The second potential surface was calculated by Viehland *et al.*[14] using the GAUSSIAN 92[18] program at the MP4SDTQ/6-311+G($2df,p$) level in the study of transport properties. The NO bond length in these calculations was fixed at $1.9392a_0$ and the potential surface had a single minimum with a depth of $6.649\times10^{-4}E_h$ at $R=5.48a_0$ and $\theta=100°$. Those MD calculations employing this potential used the NO bond length reported above, so that the calculations for each of the two potentials employed slightly different bond length values. This slight difference is taken into account when reporting angular properties by expressing results divided by the moment of inertia of the NO moiety.

Plots of the two potential surfaces for $\theta=0,\pi/2,\pi$ are shown in Fig. 1. The two potential surfaces are almost identical in the linear configurations but show more pronounced differences at the T-shaped geometry, where there is approximately a 25% difference in the depth of the potential well, and a 7% difference in the bond length. Note that over the range of field strengths employed in the present calculations, most collisions occur with relative energies in the range $1-50\times10^{-3}E_h$. Within this energy range, the difference between the two potential surfaces is much less than it is in the well region.

In order to calculate the forces and the torques needed by the molecular dynamics technique, partial derivatives of the potential surface are needed with respect to both R and $\cos\theta$. Although each of the potentials was reported as an expansion of Legendre polynomials, these expansions were not used in the present study. Instead, three uniform rectangular grids were constructed with 101 values in R spanning 2.8 to $18.9a_0$ and 41 values in $\cos\theta$ spanning -1 to 1. One grid contained the values of the potential while the other two contained the potential derivatives with respect to R and $\cos\theta$. The published analytic expressions for the potentials were used to calculate values on each of these grids which were dense enough to ensure that a simple linear interpolation scheme could reproduce the published results at any desired point in configuration space. It should be noted that the potential surface of Viehland *et al.*[14] was reported with an origin centered on the midpoint of the NO bond. In the present study, this potential was transformed to the center-of-mass of the NO moiety, consistent with the coordinate system used in the molecular dynamic code and with that reported for the Pogrebnya *et al.*[15] surface.

III. MOLECULAR DYNAMICS METHOD

In a conventional MD simulation, a system of n particles is placed within a cell of fixed volume, frequently cubic in shape, and the dimensions of the cell are chosen to satisfy the number density of the gas. A set of velocities is assigned, drawn from a Maxwell–Boltzmann distribution appropriate to the temperature of interest, with a net linear momentum equal to zero. Trajectories for all the particles are then computed by integrating the classical equations of motions. The coordinates and momenta of the particles are stored, and thermodynamic and other properties are calculated as time averages over the dynamical history of the system.

The propagator employed for all degrees of freedom in the present calculations was based upon the Verlet algorithm[19] combined with periodic boundary conditions and the cell method. The orientation of the principal body-fixed coordinate frame of the ion with respect to the space-fixed reference frame was specified with quaterions, ($\{q_i\}$, $i=1,\ldots,4$)[20,21] which satisfy the constraint $\Sigma_i q_i=1$. Quaterions are especially convenient because they remove the divergence in the transformation equations which occur at $\theta=0,\pi$ when Euler angles are used directly. The quaterions are related to the Euler angles by

$$\begin{aligned} q_1&=\sin(\theta/2)\cos((\phi-\psi)/2),\\ q_2&=\sin(\theta/2)\sin((\phi-\psi)/2),\\ q_3&=\cos(\theta/2)\sin((\phi+\psi)/2),\\ q_4&=\cos(\theta/2)\cos((\phi+\psi)/2). \end{aligned} \tag{1}$$

A common technique for integrating the rotational equations of motion employs the Gear predictor–corrector method.[21] However, in the present case, a new modified velocity Verlet algorithm was developed for the rotational motion in order to maintain the same efficiency and computational simplicity as the integration scheme used for the translational motion. In this new algorithm, the orientation of the rod at time $t+\delta t$ is calculated using

$$q_i(t+\delta t)=q_i(t)+\delta t\dot{q}_i(t)+\frac{1}{2}\delta t^2\ddot{q}_i(t),\quad i=1,\ldots,4. \tag{2}$$

At this new orientation, the forces and corresponding torques at $t+\delta t$ are evaluated, and the angular momentum, $\mathbf{L}^s$ in the space-fixed frame is advanced via

$$\mathbf{L}^s(t+\delta t)=\mathbf{L}^s(t)+\frac{1}{2}\delta t[\boldsymbol{\tau}^s(t)+\boldsymbol{\tau}^s(t+\delta t)], \tag{3}$$

in which $\boldsymbol{\tau}^s$ is the total torque acting on the ion in the space-fixed frame. Body-fixed and space-fixed quantities are related by the rotation matrix, **A**, given by

$$\mathbf{A}=\begin{pmatrix} q_1^2+q_4^2-\frac{1}{2} & q_1q_2+q_3q_4 & q_1q_3-q_2q_4 \\ q_1q_2-q_3q_4 & q_2^2+q_4^2-\frac{1}{2} & q_2q_3+q_1q_4 \\ q_1q_3+q_2q_4 & q_2q_3-q_1q_4 & q_3^2+q_4^2-\frac{1}{2} \end{pmatrix}, \tag{4}$$

so that the angular momentum and torque in the body-fixed frame are $\mathbf{L}^b=\mathbf{A}\cdot\mathbf{L}^s$ and $\boldsymbol{\tau}^b=\mathbf{A}\cdot\boldsymbol{\tau}^s$, respectively. In the body-fixed frame, $\mathbf{L}^b=\mathbf{I}\cdot\boldsymbol{\omega}^b$, where **I** is the moment of inertia tensor for a general rigid body which should be diagonal in this frame. For the present calculations, the NO^+ ion was treated as a linear rod, for which one of the diagonal elements of **I** is zero. The two nonzero angular momentum components then satisfy

$$\begin{aligned} L_x^b&=I\omega_x^b, \\ L_y^b&=I\omega_y^b, \end{aligned} \tag{5}$$

in which I is the moment of inertia of the rod. Using these relations, the angular velocity in the body-fixed frame, $\omega_i^b(t+\delta t)$, can be obtained. It can be shown[21] that

$$\dot{\mathbf{q}}=\frac{1}{2}\mathbf{W}^T\boldsymbol{\omega}^b, \tag{6}$$

in which

$$\mathbf{W}=\begin{pmatrix} q_4 & q_3 & -q_2 & -q_1 \\ -q_1 & q_4 & q_1 & -q_2 \\ q_2 & -q_1 & q_4 & -q_3 \\ q_1 & q_2 & q_3 & q_4 \end{pmatrix}, \tag{7}$$

and $\boldsymbol{\omega}^b$ is a column vector with components $[\omega_x^b,\omega_y^b,\omega_z^b,0]$. These relations are used to obtain initial estimates of $\dot{q}_i$, which in turn are used to determine $\ddot{q}_i(t+\delta t)$ from the relation

$$\ddot{\mathbf{q}}=\frac{1}{2}\mathbf{W}^T\dot{\boldsymbol{\omega}}^b, \tag{8}$$

in which $\dot{\boldsymbol{\omega}}^b$ is a column vector with components $[\dot{\omega}_x^b,\dot{\omega}_y^b,\dot{\omega}_z^b,-2\Sigma\dot{q}_i^2]$. The $\dot{\omega}_i^b$ terms are determined using the Euler equations for rigid body rotation. A typical component is given by

$$I_x\dot{\omega}_x^b=\tau_x^b+(I_y-I_z)\omega_y^b\omega_z^b. \tag{9}$$

The new part of the algorithm is the ''velocity move'' for the quaterion $\dot{q}_i$ which is completed in a manner consistent with the Verlet algorithm, that is

$$\dot{q}_i(t+\delta t)=\dot{q}_i(t)+\frac{1}{2}\delta t[\ddot{q}_i(t)+\ddot{q}_i(t+\delta t)], \tag{10}$$

and the whole procedure is repeated. Normalization of the quaterion is enforced after advancing to a new orientation to prevent gradual accumulation of numerical error.

The total force acting on the center-of-mass of the ion is given by

$$\mathbf{F}=-\sum_n \frac{\mathbf{R}_n}{R_n}\frac{\partial V}{\partial R_n}-\left[\mathbf{e}-\frac{\mathbf{R}_n}{R_n}\cos\theta_n\right]\frac{1}{R_n}\frac{\partial V}{\partial\cos\theta_n}+q\mathbf{E}, \tag{11}$$

in which $\mathbf{R}_n$ is the vector from the position of bath gas atom n to the ion center-of-mass, $R_n=|\mathbf{R}_n|$, **e** is the unit vector along the ion, q is the total charge on the ion, and **E** is the electric field applied across the drift tube. This total force is used in translating the center-of-mass of the ion and is composed of two parts. The first describes the force due to the interaction potential, $V(R_n,\cos\theta_n)$, between the ion and bath gas. The second describes the force due to the interaction of the ion with the external electric field.

The total torque acting on the ion is given by

$$\boldsymbol{\tau}^s=-\sum_n \mathbf{e}\times\frac{\mathbf{R}_n}{R_n}\frac{\partial V}{\partial\cos\theta_n}+\boldsymbol{\mu}\times\mathbf{E}, \tag{12}$$

in which $\boldsymbol{\mu}$ is the dipole moment of the ion. The first term arises from the interaction between the ion and bath gas, and has a negative coefficient due to the manner in which $\mathbf{R}_n$ is defined while the second term arises from the torque induced by the external field. In the calculation for the potential surface from Ref. 15 the value $\mu=1.360$ a.u. was used, while for the potential surface from Ref. 14 the total charge was placed at the center-of-mass resulting in the disappearance of the second term in Eq. (12). For the highest field strength employed in this study the maximum energy of the dipole electric field interaction, $\boldsymbol{\mu}\cdot\mathbf{E}$, is of the order of 1 K and thus was observed to have no effect on the mobility.

Since the ion density is very low in typical drift tube experiments, ion–ion Coulombic interactions were not included in the simulation. Furthermore within the drift tube, the ion energy acquired from the field is continuously dissipated through collisions with the bath gas which in turn transfers the heat to a thermal bath. In the MD simulations, the number of bath gas particles is of the order of 10^2 to 10^4, and an effective dissipation mechanism must be introduced to maintain the temperature of the bath gas. In the present study, a dissipation mechanism similar to that of Koutselos[5] was employed.

Specifically two simultaneous simulations are performed. In one, a pure helium bath gas is simulated using a standard constant temperature equilibrium MD method. The interaction potential between the helium atoms was chosen as a Lennard-Jones (12–6) with $\varepsilon=10.22$ K and $\sigma=4.830a_0$, and the cutoff distance for the He–He interaction was set at 8σ. After this system relaxes to equilibrium, a second simulation is started. This second simulation is initialized by placing one ion randomly in a simulation box, with dimensions matching that of the first simulation, and assigning translational and rotational velocities consistent with the equilibrium temperature of the bath gas. A sphere of radius R_{interact} is defined centered on the ion. This radius defines the distance at which ion-bath gas interactions become negligible, so that bath gas atoms at a distance greater than R_{interact} are assumed to not interact with the ion. In the present case, $R_{\text{interact}}=1.0$ nm.

The simulation boxes from these two simulations are superimposed. When a bath gas atom from the first simulation enters the interaction sphere around the ion, a copy of its position and velocity is transferred to the second simulation. The first simulation continues according to pure bath gas dynamics but the second simulation now contains a bath gas atom interacting with the ion. This system is propagated according to the ion-bath gas interaction potentials, and ion-bath gas collisions occur. Thus, the bath gas atoms from the first simulation provide initial conditions for ion-bath gas encounters in the second simulation. Once a bath gas atom in the second simulation exits the sphere of interaction, it is discarded. This is the mechanism by which bath gas energy due to the ion motion is dissipated. Physically, this implies that after bath gas atoms interact with the ion, they transfer their energy to other bath gas atoms far enough away that further interactions with the ion are not possible. This seems reasonable since the ion is constantly drifting through the bath gas, and hence encounters ''fresh'' atoms which are still in their equilibrium state.

In order to reduce computing time, only ion-bath gas interactions are treated in the second simulation, that is bath gas–bath gas interactions are ignored. This corresponds to treating the bath gas as ideal, and is justified by the low densities employed in the simulations. Note that this approximation was tested by performing simulations both with and without the bath gas–bath gas interactions. The results were identical within statistical error. Additionally, a single pure bath gas simulation can provide initial conditions for many ion simulations, so that an efficient parallel process is possible.

Summarizing, the entire procedure begins with a pure bath gas simulation. Once this first simulation reaches equilibrium, an ion simulation is initialized. This ion simulation is allowed to relax to a steady state before data is collected for statistical analysis. During the entire simulation, the thermodynamic properties of the ions and bath gas atoms are continuously monitored.

The statistical results of the MD simulation in principle can be converged, with an increase in computation time, to any predetermined accuracy. An accuracy of $\pm 1\%$ in the mobility constant was obtained by simulating 500 ions, together with a pure bath gas simulation containing 108 bath gas atoms, each with a time step of 5 fs. The bath gas was initialized in a f.c.c. lattice configuration and melted in at least 4×10^5 steps using a temperature adjustment algorithm. The ion simulations were evolved for 2×10^5 time steps in order to relax to the steady state. Finally thermodynamic averages and transport properties were accumulated for 2×10^6 steps. In all runs the number density of the buffer gas was set to $0.1\,\mathrm{nm}^{-3}$. During the accumulation period the number of ion–atom collisions for the entire ensemble of ions was in the range $2.5–6.5\times10^6$ depending upon electric field strength.

IV. RESULTS

A. Mobility

The mobility, κ, of a gas phase ion is defined by $\kappa = v_D/E$, in which v_D is the drift velocity. The mobility is a measure of the rapidity with which an ion moves through a buffer gas under the influence of a uniform electric field. In the simulations, the drift velocity is calculated using

$$v_D = \overline{\langle v_\parallel \rangle}, \tag{13}$$

in which $\langle \cdots \rangle$ denotes a steady state ensemble average, the bar denotes a time average over the total simulation, and $v_\parallel$ is the ion velocity in the direction parallel to the electric field. To estimate the variance in the statistical quantities, standard block analyses were performed.[22] Since the mobility depends upon the buffer gas number density, reduced mobilities scaled to the number density at standard pressure and temperature are used. The reduced mobility, κ_0, can be obtained from the measured or calculated drift velocity using the relation

$$\kappa_0 = \frac{v_D}{E/N}\frac{1}{N_0}, \tag{14}$$

in which $N_0 = 0.026868\,\mathrm{nm}^{-3}$. Mobilities are expressed as a function of the reduced field strength E/N in units of Td, $(1\,\mathrm{Td} = 10^{-21}\,\mathrm{V\,m^2})$.

Reduced mobilities using each of the two interaction potentials are compared in Table I. Within statistical error, the results from the two potentials are identical. This is consistent with the similarity of the two surfaces in the repulsive wall region in the energy range which the trajectories sample, as seen in Fig. 1, and indicates that the well regions, for which there are more substantial differences, contribute little to the mobility. The mobilities are compared with the calculated results of Viehland *et al.*[14] and the experimental results of de Gouw *et al.*[16] in Fig. 2. All the results agree to within statistical error except for field strengths very close to zero. In this regime, the MD method is slow to converge because the drift velocity is very small. Thus, the error bars in the present MD results are quite large. Even so, the MD results seem to approach a limiting value of about $22\,\mathrm{cm^2/V\,s}$ at zero field while those of Viehland *et al.* approach $22.5\,\mathrm{cm^2/V\,s}$. In this latter work, the authors state that their method had difficulty converging the results at their highest recorded field strengths. The MD method employed here, however, converges quite nicely with larger fields and results up to 200 Td have been converged without any difficulties. This wide range of coverage allows comparisons with all the measured values of de Gouw *et al.*[16]

In addition to reduced mobilities, Table I also compares the average squared velocities parallel and perpendicular to the field, with the latter defined as

$$\langle v_\perp^2 \rangle = \frac{1}{2}(\langle v_x^2 \rangle + \langle v_y^2 \rangle), \tag{15}$$

in which the z direction was chosen as the direction of the field. In a gas at thermal equilibrium these two quantities should both be equal to kT/m with m the mass of the ion and k the Boltzmann constant. As with the reduced mobilities, Table I shows that the drift velocities, and squared velocities are essentially the same within statistical errors for the two potential surfaces.

TABLE I. Reduced mobilities, drift velocities, and values of $\langle v_{\parallel}^2 \rangle$ and $\langle v_{\perp}^2 \rangle$ for NO^+ drifting in helium at 300 K for several values of E/N, as determined by molecular dynamics simulation. A: potential surface of Viehland *et al.*,[a] B: potential surface of Pogrebnya *et al.*[b] The standard deviation is about 1% (for $E/N=1.0$ Td about 3%).

	κ_0 (cm^2/V s)		v_D (nm/ps)		$\langle v_{\parallel}^2 \rangle$ ([nm/ps]^2)		$\langle v_{\perp}^2 \rangle$ ([nm/ps]^2)	
E/N (Td)	A	B	A	B	A	B	A	B
1.0	21.92	21.92	0.059	0.059	0.0863	0.0871	0.0827	0.0834
5.0	22.35	22.08	0.300	0.297	0.179	0.177	0.0860	0.0850
10.0	22.19	21.87	0.596	0.588	0.463	0.452	0.0949	0.0950
15.0	21.79	21.81	0.878	0.879	0.906	0.909	0.1080	0.1082
20.0	21.49	21.40	1.155	1.150	1.50	1.49	0.1258	0.1262
25.0	21.00	20.96	1.410	1.408	2.20	2.19	0.146	0.146
30.0	20.55	20.54	1.656	1.656	2.95	3.00	0.169	0.169
35.0	19.96	20.07	1.877	1.887	3.82	3.86	0.193	0.196
40.0	19.47	19.55	2.092	2.101	4.71	4.76	0.217	0.219
45.0	18.92	18.98	2.288	2.294	5.62	5.64	0.245	0.246
50.0	18.43	18.52	2.476	2.488	6.56	6.62	0.272	0.273

[a]Reference 14.
[b]Reference 15.

B. Velocity autocorrelation functions, diffusion coefficients, and averages of the angular momentum–alignment parameters

The transport of ions in a mobility experiment results from a steady state drift part and a diffusional motion part. In order to characterize the latter, diffusion coefficients parallel and perpendicular to the electric field were calculated, employing an approach based upon the integration of velocity autocorrelation functions. If for each ion, a velocity difference is defined, $\Delta \mathbf{v}_i(t)=\mathbf{v}_i(t)-\langle \mathbf{v} \rangle$, then

$$\mathbf{C}(t)=\langle \Delta \mathbf{v}_j(t) \cdot \Delta \mathbf{v}_j(0) \rangle, \tag{16}$$

is the unnormalized velocity autocorrelation function and

$$\mathbf{D}=\int_0^{\infty} \mathbf{C}(t)dt, \tag{17}$$

defines the diffusion tensor. In the present work, $D_{\parallel}=D_{zz}$ and $D_{\perp}=(D_{xx}+D_{yy})/2$. The ion velocity correlation functions, $\mathbf{C}(t)$, are determined using the multiple time origins method,[19] and the times for which the data are collected give an accuracy of about 2%.

Normalized correlation functions, $C_{\parallel}$ and $C_{\perp}$ are presented in Fig. 3 for the potential surface of Pogrebnya *et al.*[15] The long tails on the correlation functions are characteristic of the ion–atom mass ratio and the low density of the system. As the electric field increases, the correlation functions decay more quickly, as a result of the higher number of ion-bath gas collisions. At short times, the shape of the correlation functions is consistent with that of free ion motion. At long times, the correlation functions decay exponentially and there is an increase in the relative error. Thus, in integrating the correlation function, an exponential fit was employed for times larger than 400 ps and the integration from this time to infinity was performed analytically. In the region from 0 to 400 ps the correlation functions were integrated numerically. The resulting ion-diffusion coefficients for both potential surfaces are reported in Table II. Once again the diffusion coefficients for both potential surfaces are essen-

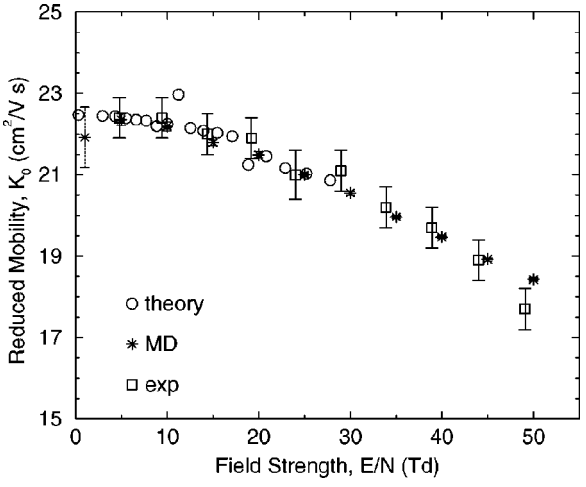

FIG. 2. Reduced mobility, κ_0, as a function of E/N for NO^+ drifting in helium at 300 K. Open circles represent results of Ref. 14, stars represents MD results, and open squares represent experimental data from Ref. 16.

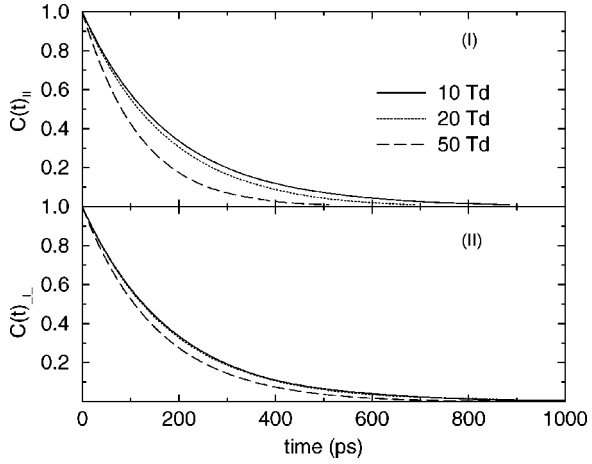

FIG. 3. Velocity autocorrelation functions, $C_{\parallel}(t)$—(I) and $C_{\perp}(t)$—(II), for NO^+ drifting in helium at 300 K, at various field strengths.

TABLE II. Values of $ND_{\|}$, $ND_{\perp}$, $\langle J_{\|}^2\rangle$, and $\langle J_{\perp}^2\rangle$ for NO^+ drifting in helium at 300 K for several values of E/N, as determined by molecular dynamics simulation. (A) potential surface of Viehland *et al.*,[a] (B) potential surface of Pogrebnya *et al.*[b] The standard deviation is about 2% for the diffusion coefficients and about 1% for the angular momentum averages.

	$ND_{\|}$ $10^{18}(\mathrm{cm\,s})^{-1}$		$ND_{\perp}10^{18}(\mathrm{cm\,s})^{-1}$		$\langle J_{\|}^2\rangle/2Ik_B$ (K)		$\langle J_{\perp}^2\rangle/2Ik_B$ (K)	
E/N (Td)	A	B	A	B	A	B	A	B
1.0	15.57	15.47	15.38	15.41	100.7	100.9	100.1	99.9
5.0	15.83	16.69	15.78	15.58	103.9	104.4	105.2	104.7
10.0	19.84	20.04	17.65	17.47	114.9	113.6	122.3	121.0
15.0	23.19	24.24	19.56	19.75	131.1	130.8	147.4	146.8
20.0	27.69	28.20	22.72	22.59	154.2	154.9	178.4	177.6
25.0	33.83	32.26	23.39	25.73	177.9	184.3	216.3	214.4
30.0	35.44	37.14	29.32	28.86	208.8	205.9	251.3	253.8
35.0	39.56	40.33	32.95	32.99	233.8	239.0	295.5	301.6
40.0	43.30	43.78	36.70	35.56	265.0	270.3	332.4	345.4
45.0	44.96	46.28	38.15	39.35	292.6	301.3	375.8	386.3
50.0	46.82	49.84	41.02	41.87	325.5	330.9	419.7	428.1

[a]Reference 14.
[b]Reference 15.

tially the same, and agree to within 5%. They are also in good quantitative and qualitative agreement with the results reported by Viehland *et al.*[14] at low electric fields and contain much less scatter for field strengths above 20 Td.

In the same table we present the averages of the angular momentum components in the directions parallel, $\langle J_{\|}^2\rangle = \langle J_z^2\rangle$, and perpendicular, $\langle J_{\perp}^2\rangle = (\langle J_x^2\rangle + \langle J_y^2\rangle)/2$, to the field, scaled by the moment of inertia of the molecule (to remove the difference in equilibrium bond length for the two potentials). The results for both potential surfaces are the same within the range of standard deviation. For field strengths above 30 Td the results agree within 2% which suggests that the overall asymmetry for both potential surfaces is the same, again consistent with the plots in Fig. 1. It is interesting to note that the rotational energy,

$$E_{\mathrm{rot}} = \frac{1}{2I}(\langle J_x^2\rangle + \langle J_y^2\rangle + \langle J_z^2\rangle), \tag{18}$$

is not equally partitioned between the parallel and perpendicular directions, and this suggests some degree of orientation and alignment of the ion during the drifting motion. In their classical trajectory calculations, Viehland *et al.*[14] noted the poor convergence of $\langle J_{\perp}^2\rangle$ and $\langle J_{\|}^2\rangle$ values even at low fields. In contrast, the values of the present calculations are well converged. Furthermore in the MD simulation there are no explicit assumptions about the odd powers of the components of the angular momentum and within numerical uncertainty they were found to average to zero. Thus, the simulation is reproducing the expected analytical results in this case as well since the relation

$$\langle J_{\perp}\rangle = \left\langle \frac{1}{2}(J_x + J_y)\right\rangle = 0, \tag{19}$$

reflects the axial symmetry about the electric field, and

$$\langle J_{\|}\rangle = \langle J_z\rangle = 0, \tag{20}$$

reflects the fact that there is no preferred orientation for the molecule as it drifts.

Following Orr-Ewing and R. Zare,[23] the alignment parameter $A_0^{(2)}$ is defined as

$$A_0^{(2)} = 2\langle P_2(\hat{\mathbf{J}}\cdot\hat{\mathbf{z}})\rangle, \tag{21}$$

in which $P_2(x)$ is a Legendre polynomial and $\hat{\mathbf{J}}$ is an unit vector along $\mathbf{J}$. This parameter has a numerical value between $+2$ (when $\mathbf{J}$ lies along $\hat{\mathbf{z}}$) and -1 (when $\mathbf{J}$ lies perpendicular to $\hat{\mathbf{z}}$). The results of the alignment parameter for both potential surfaces are presented in Fig. 4. Once again, the two potential surfaces produce the same alignment values. At low fields where the ion motion is only slightly perturbed from thermal equilibrium no alignment is detected. However, with increasing field strength, the ion shows a tendency to rotate in a plane parallel to the direction of the field. To determine whether the alignment saturates at even larger fields we plan to perform calculations in the future up to 200 Td.

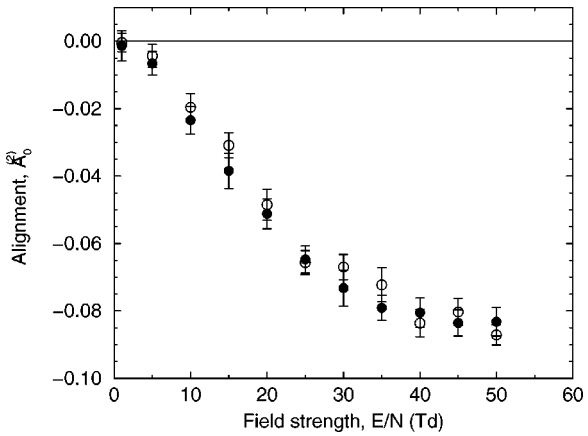

FIG. 4. Calculated alignment parameter $A_0^{(2)}$ as a function of E/N for NO^+ drifting in helium at 300 K. Filled and open circles represent results for the potential surfaces of Refs. 14 and 15, respectively.

V. CONCLUDING REMARKS

A new molecular dynamics method is introduced which can simulate the drifting of a general rigid ion in a buffer gas. This method is utilized in calculating mobilities of NO^+ drifting through helium at 300 K for values of E/N varying from 0 to 50 Td. We have performed calculations for two different *ab initio* NO^+–He potential surfaces[14,15] and found that within numerical uncertainties both potentials yield essentially the same values for mobilities, diffusion coefficients, and alignment parameters. The potential surfaces are similar but do show substantial differences in well depth near T-shaped geometries. However, these differences do not manifest themselves in either the mobility or alignment parameters because the relative collision energies in the present calculations sample points higher up on the repulsive wall where the two surfaces are fairly similar.

The mobility values are in good agreement with recent theoretical calculations of Viehland *et al.*[14] and with experimental data of de Gouw *et al.*[16] This substantiates the validity of the MD method. In a subsequent paper, a variety of distributions functions will also be examined in order to show the level of detail which the MD method can provide. Our intent is to use this method to study much larger and more complex ions, especially those of biological interest. The current study has shown that the proposed MD method describes correctly the chemistry and physics of the mobility experiment.

ACKNOWLEDGMENTS

We would like to thank S. Pogrebnya for sending us a FORTRAN subroutine coding their potential surface. We would also like to thank Professor Don Douglas for helpful discussions. This work was supported by a Grant from the Natural Sciences and Engineering Research Council of Canada.

[1] E. A. Mason and E. W. McDaniel, *Transport Properties of Ions in Gases* (Wiley, New York, 1988).
[2] L. A. Viehland, Chem. Phys. **101**, 1 (1986).
[3] H. Skullerud, J. Phys. B **6**, 728 (1973).
[4] S. N. Lin and J. N. Bardsley, J. Chem. Phys. **66**, 435 (1977).
[5] A. D. Koutselos, J. Chem. Phys. **102**, 7216 (1995).
[6] M. F. Jarrold, J. Phys. Chem. **99**, 11 (1995).
[7] M. F. Mesleh, J. M. Hunter, A. A. Shvartsburg, G. C. Schatz, and M. F. Jarrold, J. Phys. Chem. **100**, 16082 (1996).
[8] S. Lee, T. Wyttenbach, G. von Helden, and M. T. Bowers, J. Am. Chem. Soc. **117**, 10159 (1995).
[9] T. Wyttenbach, G. von Helden, and M. T. Bowers, J. Am. Chem. Soc. **118**, 8355 (1996).
[10] T. Covey and D. Douglas, J. Am. Soc. Mass Spectrom. **4**, 616 (1996).
[11] B. A. Collings and D. J. Douglas, J. Am. Chem. Soc. **118**, 4488 (1996).
[12] L. A. Viehland and A. S. Dickinson, Chem. Phys. **193**, 255 (1995).
[13] H. Meyer and S. R. Leone, Mol. Phys. **63**, 705 (1998).
[14] L. A. Viehland, A. S. Dickinson, and R. G. A. R. Maclagan, Chem. Phys. **211**, 1 (1996).
[15] S. K. Pogrebnya, A. Kliesch, D. C. Clary, and M. Cacciatore, Int. J. Mass Spectrom. Ion Processes **149/150**, 207 (1995).
[16] J. A. de Gouw, L. N. Ping, M. Krishnamurthy, H. S. Lee, E. B. Anthony, V. M. Bierbaum, and S. R. Leone, J. Chem. Phys. **105**, 10398 (1996).
[17] V. A. Zenevich, W. Lindinger, S. K. Pogrebnya, M. Cacciatore, and G. D. Billing, J. Chem. Phys. **102**, 6669 (1995).
[18] J. B. Foresman and Æ. Frisch, *Exploring Chemistry with Electronic Structure Methods: A Guide to Using Gaussian* (Gaussian Inc., Pittsburgh, 1993).
[19] M. P. Allen and D. J. Tildesley, *Computer Simulation of Liquids* (Oxford University, Oxford, 1994).
[20] H. Goldstein, *Classical Mechanics* (Adison-Wesley, London, 1959).
[21] D. C. Rapaport, *The Art of Molecular Dynamics Simulation* (Cambridge University, Cambridge, 1995).
[22] D. Frenkel and B. Smit, *Understanding Molecular Simulation From Algorithms to Applications* (Academic, San Diego, 1996).
[23] A. J. Orr-Ewing and R. N. Zare, Annu. Rev. Phys. Chem. **43**, 315 (1994).